Journal of Molecular Liquids 391 (2023) 123365

Contents lists available at ScienceDirect

Journal of Molecular Liquids

journal homepage: www.elsevier.com/locate/molliq

Phase behavior of phospholipid-based myelin figures influenced by pH

D. Benkowska-Biernacka [a], I.I. Smalyukh [b,c], K. Matczyszyn [a,c,*]

[a] Institute of Advanced Materials, Faculty of Chemistry, Wroclaw University of Science and Technology, 50-370 Wroclaw, Poland
[b] Department of Physics and Materials Science and Engineering Program, University of Colorado Boulder, Boulder, CO 80309, United States
[c] International Institute for Sustainability with Knotted Chiral Meta Matter (WPI-SKCM^2), Hiroshima University, Higashihiroshima, Hiroshima 739-8526, Japan

ARTICLE INFO

Keywords:
Lipidic mesophases
Lyotropic liquid crystals
Lipid phase transition temperature
Polarized light microscopy
Confocal fluorescence microscopy
Two-photon excited fluorescence microscopy

ABSTRACT

The study of the effects of external stimuli on lipidic mesophases may enable a better understanding of alterations in biomembranes and improve the design of multilayered lipid structures. Here we demonstrate the influence of pH on the formation of elongated multilamellar assemblies, known as myelin figures (MFs). Polarized light microscopy allowed us to follow the growth process and thermal stability of phosphatidylcholine-based MFs. Our results reveal that the dimensions of these cylindrical microstructures change depending on the initial pH of the aqueous phase required for the self-assembly of lipids into MFs. Furthermore, we have confirmed the significant strength of the association between pH and characteristic parameters of MFs using Spearman's rank correlation tests. Also, we have shown that one- and two-photon fluorescence microscopy can reveal the morphological changes that occur in MFs resulting from the lipid phase transition. These findings indicate the feasibility of using non-destructive methods to gain insight into liquid crystalline properties of biologically relevant multilamellar lipid structures in a wide pH range.

1. Introduction

An important aspect of soft matter research is the development of new approaches to better understand the properties and functions of biologically relevant structures [1–3]. Liquid crystalline phases are observed in normal and lesioned tissues related to various pathologies that introduce or modify the mesomorphic states [4–6]. Among nature-inspired mesophases, myelin figures (MFs) resemble a lipid-rich (70–85% of dry weight) native membrane, which insulates the axon and facilitates the conduction of an action potential [7,8]. The defects and disruptions in multilamellar lipid assembly within the myelin sheath cause less efficient transmission of nerve impulses [9,10]. Interdisciplinary studies on biomimetic membranes may provide new perspectives for *in vivo* imaging of small-scale morphological changes associated with myelin disorders of incompletely understood origin (e.g., multiple sclerosis) [4,11,12].

Lipid molecules contain spatially distinguishable hydrophilic (polar headgroup) and hydrophobic (hydrocarbon chains) parts. Depending on geometrical parameters, amphiphile concentration, and environmental conditions, lipids may self-assemble into different well-defined forms in an aqueous medium [13–15]. At considerably high concentrations, lipids can organize into three-dimensional (3D) multilamellar assemblies, i.e., in spherical and cylindrical shapes [16,17]. Purely lipidic MFs are elongated 3D forms that consist of hundreds of concentrically wrapped lipid bilayers interspaced with layers of water [7,18,19]. These structures are formed above the main phase transition temperature (T_m), where lipids are in the liquid crystalline phase. Under these conditions, the hydrocarbon chains are disordered as a result of the *trans*-gauche isomerization of some of the C–C bonds. Below T_m, lipids are in an ordered gel phase, the polar headgroups are tightly packed, and all C–C bonds within the acyl chains are in the trans configuration [20–23].

The phase behavior of lipid bilayers may respond to external stimuli such as variations in pH [24], temperature [25,26], and ion strength [27]. The effect of localized pH fluctuations on membrane-related issues has been of great interest, for example, in the context of neuronal activity [28–30], erythrocyte deformability [31], and specific drug release

Abbreviations: 2PEFM, two-photon excited fluorescence microscopy; 3D, three-dimensional; CFM, confocal fluorescence microscopy; DLPC, 1,2-dilauroyl-*sn*-glycero-3-phosphocholine; DMPC, 1,2-dimyristoyl-*sn*-glycero-3-phosphocholine; DSC, differential scanning calorimetry; MFs, myelin figures; PCs, phosphatidylcholines; PLM, polarized light microscopy; r_s, Spearman's rank correlation coefficient; RT, room temperature; SAXS, small - angle X-ray scattering; T_m, phase transition temperature.

* Corresponding author at: Institute of Advanced Materials, Faculty of Chemistry, Wroclaw University of Science and Technology, 50-370 Wroclaw, Poland.
E-mail addresses: dominika.benkowska@pwr.edu.pl (D. Benkowska-Biernacka), ivan.smalyukh@colorado.edu (I.I. Smalyukh), katarzyna.matczyszyn@pwr.edu.pl (K. Matczyszyn).

https://doi.org/10.1016/j.molliq.2023.123365
Received 4 July 2023; Received in revised form 29 September 2023; Accepted 16 October 2023
Available online 18 October 2023

[32,33]. Previous studies have shown that acidic pH may increase T_m of phospholipids due to the protonation of the phosphate group, causing enhanced hydrogen bonding between adjacent headgroups [34–36]. Since T_m is an important factor to control the stability of membranes [37], it has been probed with various experimental methods. Those include differential scanning calorimetry (DSC) [35,36,38], small-angle X-ray scattering (SAXS) [39], atomic force microscopy [25], fluorescence spectroscopy [24,40], nanoplasmonic sensing [41] and others [42,43].

Considering the lipid composition of the myelin sheath, the present study focuses on MFs composed of phosphatidylcholines (PCs), a class of phospholipids commonly found in biomembranes [10,44–46]. PCs have a zwitterionic headgroup that contains a positively charged quaternary amine and a negatively charged phosphate group. The single-component lipid systems in the shape of vesicles have been extensively studied as simple models of biological structures, while there is much less research on multilamellar microstructures in the shape of cylinders. Several studies have described the effect of external factors on the formation and morphology of MFs [19,47–52]. For example, the elongation growth rate of multilayered lipid tubes could be increased by thermal [53] and hydration gradients [54,55]. The use of digital holographic microscopy has shown that the formation of unsaturated PC-based MFs at room temperature (RT) can be influenced by pH of the surrounding medium [56].

Here we study the correlation between pH and phase behavior of saturated PC-based MFs with different T_m by methods commonly applied to examine liquid crystalline phases. The thermal stability and growth process of multilamellar lipid tubes are precisely followed over a wide range of pH values. Insights into the characteristic parameters of MFs are provided using polarized light microscopy (PLM), showing that MFs can form without shape disruption under extreme pH conditions above T_m. In addition, we use one- and two-photon microscopy with temperature control to characterize the morphological changes along the Nile Red-stained MFs caused by the transition from the liquid crystalline to the gel phase. The use of PLM and fluorescence imaging techniques allows us to determine the organization of lipid molecules within multilamellar structures. Despite extensive research on lipid assemblies, we present the first study on PC-based MFs using polarization-sensitive two-photon fluorescence excited microscopy.

2. Experimental

2.1. Chemicals

Synthetic phospholipids, 1,2-dilauroyl-*sn*-glycero-3-phosphocholine (DLPC) and 1,2-dimyristoyl-*sn*-glycero-3-phosphocholine (DMPC) were purchased from Avanti Polar Lipids. Phospholipids were dissolved in chloroform (spectrophotometric grade). The fluorescent dye, 9-Diethylamino-5H-benzo[α]phenoxazine-5- one (Nile Red), was purchased from Biotium. The pH of the aqueous phase was adjusted by adding the appropriate amount of HCl or NaOH to Milli-Q water.

2.2. Sample preparation

MFs were prepared from a single type of phospholipid (DLPC or DMPC). First, a certain amount of PCs was dissolved in chloroform to prepare a solution of 20 mg/mL. Then a small drop of the lipid solution was placed on a coverslip. The sample was left to evaporate under a vacuum overnight. After that, a liquid crystal cell was prepared using spacers with a diameter of 30 μm and a coverslip to cover the dry lipid droplet. The as-obtained sample was placed on a heating stage set at 20 °C and hydrated with the solution at a specified pH using capillary forces. The pH was controlled by a Mettler Toledo pH meter.

2.3. Characterization of myelin figures

The samples without the fluorescent dye were observed by the Olympus BX60 optical microscope equipped with two crossed polarizers and a 530 nm full-wave retardation plate. A temperature-controlled Linkam LTS120 stage was used to cool or heat the samples to a desired temperature within 0.1 °C with a 0.5 °C/min ramp. Experiments that followed the formation of MFs over time were carried out using a Pixel TC-252 intervalometer.

Confocal fluorescence microscopy (CFM) was carried out using the Olympus IX83 equipped with a 488-nm diode laser. Two-photon excited fluorescence microscopy (2PEFM) was performed using the Olympus IX81 with a femtosecond laser system (Ti: Sapphire oscillator, Chameleon Ultra II, Coherent Inc., 140 fs, 80 MHz repetition rate) [57]. The fluorescence signal was spectrally separated by a dichroic mirror (570 nm) and sent through a 610/75 nm band pass filter (Semrock) and a 720 nm short pass filter (Semrock) to minimize the collection of undesired signals. The bright-field and polarized-light optical images were captured by a charge-coupled device camera (Grasshopper, Point Grey Research).

All fluorescence microscopy studies were conducted on MFs stained with Nile Red using inverted microscopes. The emission signals were epi-collected by high numerical aperture oil immersion objectives, the same as used for excitation (60x/1.35 and 100x/1.40). Temperature-dependent experiments employed the objective heater controller (Bioptech) with an accuracy of 0.1 °C. Image analysis was performed using the Olympus Fluoview and ImageJ software.

2.4. Statistical analysis

The statistical strengths of nonlinear monotonic relationships were determined by evaluating Spearman's rank correlation coefficient (r_s). The p values were calculated to show the probability of observing those strengths of association. Both parameters were interpreted according to commonly accepted standards. The strength of correlation increases as absolute values of r_s in the range of 0–1, while p values below 0.05 indicate a statistically significant test result [58,59].

3. Results and discussion

3.1. The pH effect on the temperature of the MFs formation

Firstly, PLM was used to observe the growth and stability of phospholipid-based MFs prepared according to the contact method [55]. After the hydration above the T_m, the cylindrical multilamellar structures start to grow from the edge of the concentrated surfactant plaques toward the isotropic phase (Fig. 1a) [7,55]. Recent studies showed that the formation of MFs should be considered in terms of thermal and hydrodynamic manipulation [60]. To preliminarily determine the effect of initial conditions on the growth process of MFs, the experiments were performed on samples with DMPC, which exhibit T_m around 24 °C.

Inserting a full-wave retardation plate between two polarizers enhances the contrast between the different parts of the MFs and the background. This enabled us to detect thinner structures, such as those with fewer phospholipid bilayers. Furthermore, the colors introduced by the additional optical element reveal the differences along the multilamellar tubes. The blue and yellow interference colors in polarized light micrographs indicate regions where the aliphatic tails of the phosphatidylcholines are oriented parallel and perpendicular to the slow axis of the waveplate, respectively.

Subsequently, to determine the average temperature at which MFs begin to form under different pH conditions, a series of experiments were carried out using a polarized light microscope equipped with the full-wave retardation plate. Samples were wetted with an aqueous solution of a specified pH ranging from 1 to 13. The tests for each sample started with a 5-min incubation at 20 °C, followed by an increase in the

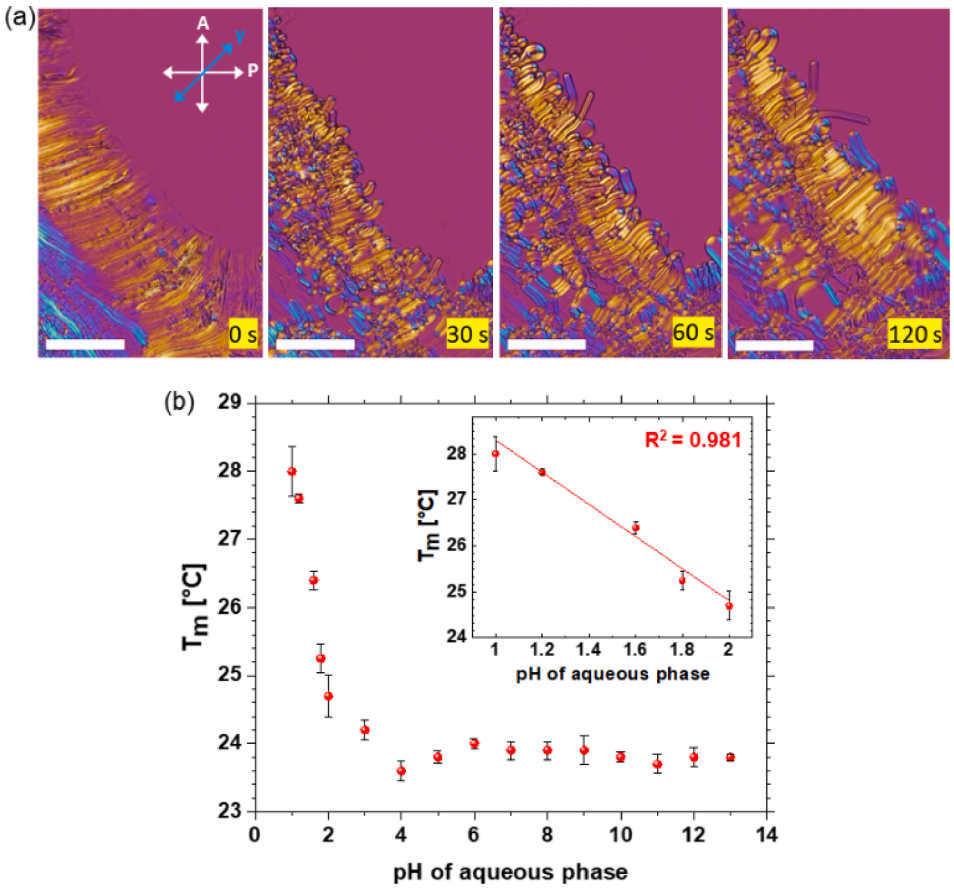

Fig. 1. (a) Polarized light micrographs showing the growth of DMPC-based MFs 0 s, 30 s, 60 s, and 120 s after the addition of aqueous media of pH 6 at 24 °C. White arrows correspond to crossed polarizers (A – analyzer, P – polarizer), while the blue arrow indicates the slow axis of the full-wave retardation plate (γ). Scale bars represent 100 μm. (b) Evolution of the phase transition temperature vs. pH values of the aqueous environment for DMPC-based MFs. The inset illustrates a zoom-in of the same plot in a narrow pH range (1–2).

incubation temperature with a step of 0.5 °C/min. Below T_m, there was no self-assembly of lipids in vesicles or tubes, whereas above T_m, the rapid formation of elongated microstructures was noted at the edge of the lipid droplet (Fig. S1†). The presence of MF's unique forms (i.e., straight, round and twisted) was not observed to be affected by the change of the pH values of the aqueous medium. Furthermore, the phase transition along the representative DMPC-based MFs could be reversed without material loss by cooling and heating the as-prepared tubular structures through T_m, as demonstrated in Fig. S2†.

The results shown in Fig. 1b reveal a tendency for the T_m to increase as the pH of the solution decreases, particularly in strongly acidic environments. It has been noted that the T_m rises as the acidic character of the isotropic phase increases (particularly from pH 3 to lower values). In the pH range from 1 to 2, the number of measurement points was taken due to the pronounced change in T_m with reference to the T_m at pH 7 ($\Delta T_{pH\ 1\text{-}pH\ 7} = \sim 3.3$ °C). Under these strongly acidic conditions, the linear dependence of T_m on pH was observed. Whereas T_m in the pH range between 4 and 13 remains roughly the same, the fluctuation is within 1 °C. The Spearman rank correlation analysis confirmed that T_m and pH are negatively correlated over the entire measurement range ($r_s = -0.8$ and p value < 0.001). The strength of the association between these two variables was determined as strong.

Additionally, we followed the T_m of DMPC-based multilamellar vesicles formed in acidic, neutral, and alkaline media by DSC (see SI). As shown in Fig. S3†, the phase transition peaks upon heating were noted at ~ 25.0, 23.7, and 23.4 °C in samples prepared at pH 2, 7, and 13. Similar results were obtained in the experiments performed by PLM to examine the formation of DMPC-based MFs, the T_m were at ~ 24.7, 23.9, and 23.8 °C, respectively. These findings differ slightly from those previously reported for the dispersion of DMPC-based liposomes by DSC [36], probably due to different experimental parameters. In our study, we set a lower heating and cooling rate to reduce the thermal gradient effect (0.5 °C/min instead of 3 °C/min). By means of DSC and PLM, we observed the same trend in T_m at low pH, except that the thermal stability of the lipids began to alter substantially from pH 3 (instead of 2), and the T_m reached lower values.

The relationship between T_m and pH can be explained by the protonation and deprotonation of functional groups within the PC headgroup. At low pH, the phosphate group is protonated ($pK_a < 2$), resulting in an increase in electrostatic repulsion between adjacent positively charged headgroups and enhanced hydrogen bonding between the neighboring lipids. The PC headgroup is zwitterionic at neutral pH since the quaternary ammonium group expects to be neutralized only under extremely alkaline conditions (pH > 12) [34,36,61,62].

3.2. The pH effect on the growth process and dimensions of MFs

Then, we followed the formation of the myelinic organization over time to assess how various pH conditions affect the growth process of MFs. The samples were hydrated at the T_m, and images were taken every 5 s for 150 s. To quantify the growth behavior of MFs, five straight tubes showing undisturbed elongation (i.e. not encountering obstacles and presenting regular morphology) were selected at different pH of the aqueous phase (1, 2, 7, 9 and 13) and measured from roots to tips. Firstly, the rapid rate of MFs' elongation was observed, and then a process of slowing down the formation of MFs was noted over the entire

range of tested pH values. As illustrated in Fig. 2a, MFs' growth curve over a wide pH range can be successfully approached by typical diffusion behavior [63,64], where the length of a lipid tube (l) is directly proportional to the square root of time (t). Such dependence is characteristic for lyotropic MFs, after the initial seconds of rapid growth, and is caused by a hydration gradient within the region of lipid-water interface [65–67]. Fig. 2b depicts that the growth rate remained fairly constant 60 s after sample hydration. The length increments (Δl) were approximately 40%, 27%, and 26% of the initial value (i.e. within 15 s after sample preparation) for pH 1, 7, and 13, respectively. Furthermore, longer multilamellar structures were formed in acidic than in neutral pH, and vice versa in alkaline pH. The differences in growth curves between multilamellar lipid tubes obtained at various pH can result from changes in H^+/OH^- concentrations, which lead to alterations in interfacial tension of lipid membrane [56,68].

The mean diameters of DMPC-based MFs observed 150 s after sample preparation at different pH are shown comparatively in Fig. 2c. The diameters of the MFs ranged from 20.1 μm ± 4.4 μm (pH 1) to 8.2 μm ± 3.62 μm (pH 13), depending on the pH of the aqueous phase. The Spearman rank correlation coefficient ($r_s = -0.7$ and p value < 0.001) confirmed the strong association between diameter and pH. As the coefficient is negative, there is a decrease in the MF diameter with an increase in the pH of the aqueous phase. The increase in the diameter at low pH can be caused by the dehydration of the PC headgroup in acidic media, resulting in a decreased headgroup area and thickening of the lipid bilayers [35,69]. To monitor changes in the width of the elongated multilamellar structures during the growth process, it was assumed that the MFs were cylindrical, with no cavities or bulges along their length. Fig. S4 † shows that even if the length of the MFs increases, its diameter remains the same along the tube. As shown in Fig. 2d-f, the characteristic arrangement of the phospholipids in the stacks of bilayers wrapped around the water channel running along the entire structure does not change over tested conditions. The long axes of the DMPC molecules for each sample are oriented perpendicularly to the flow direction of the aqueous core, except for the MF tip.

Another aspect to consider is whether the relationship between the diameters of MFs and pH is applied when measurements are performed at the same initial temperature. Therefore, further experiments were conducted on DLPC-based MFs formed in the water phase of pH 1, 7 and 13 at 25 °C, well above its T_m ($T_{m\ DLPC} = -2$ °C). The results in Fig. 2g

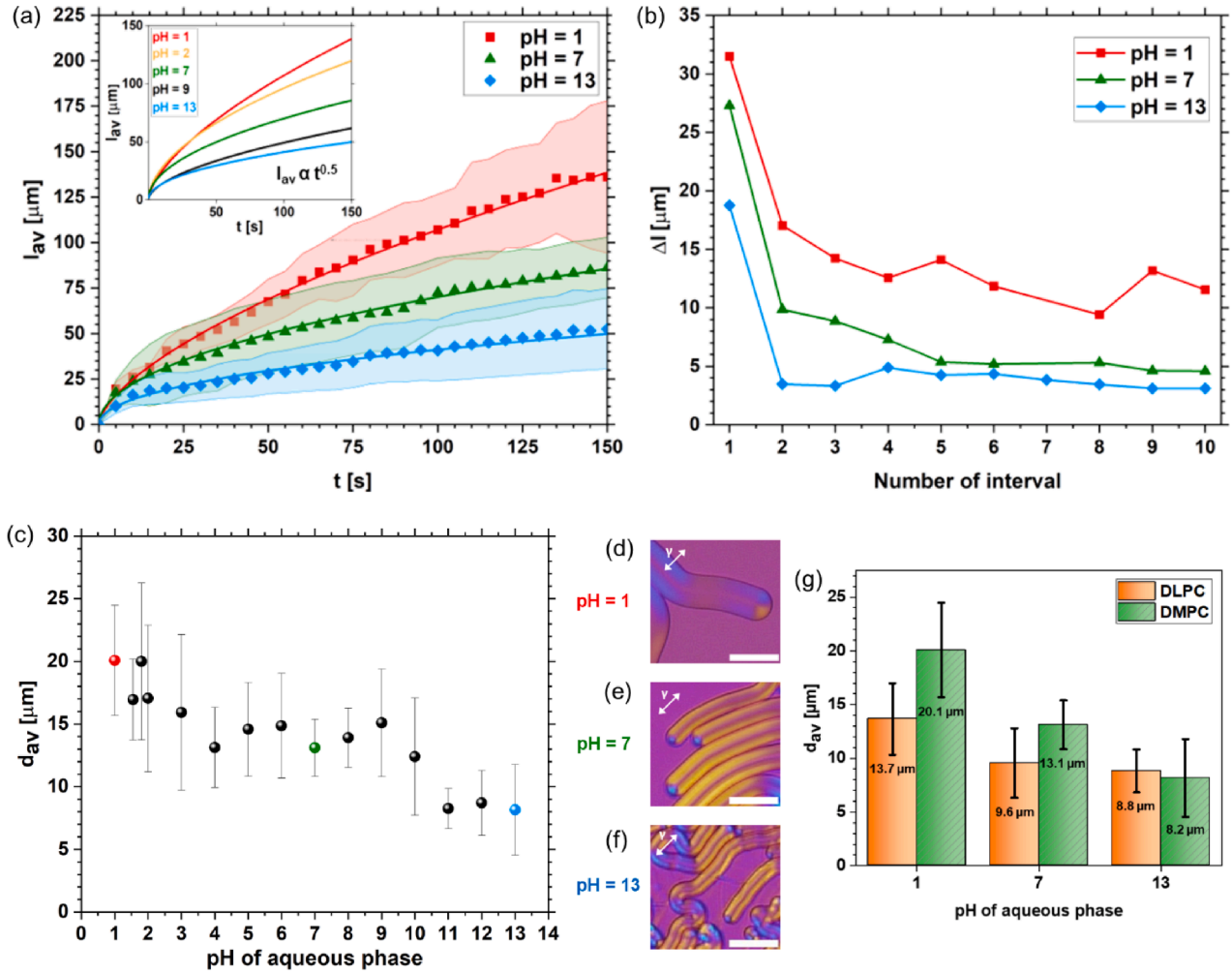

Fig. 2. (a) Growth curves of MFs formed under different pH conditions at the phase transition temperatures. The shaded error bands correspond to the standard deviation of the mean MF length (l_{av}) measured for five representative cylindrical structures after a certain time from the start of growth (t). The insert demonstrates the fitted growth curves over a wide pH range. The pH of aqueous media was adjusted to 1 (red squares and lines), 2 (yellow line), 7 (green triangles and lines), 9 (black line), and 13 (blue inverted squares and lines). (b) The plot shows the tube length increment (Δl) in 15-second intervals. (c) Plot showing the average diameter of MFs (out of 60 measurements) vs. the pH of the aqueous phase. (d-f) Representative polarized light images of pristine MFs performed after the addition of (d) acidic, (e) neutral and (f) alkaline solution. The white double arrows show the orientation of the slow axis of the retardation plate. Scale bars correspond to (d-f) 30 μm. (g) The representative average diameters of MFs composed of DLPC (orange, plain pattern) at 24 °C or DMPC (green, diagonal pattern) at T_m; lipids were dissolved in chloroform, dried, and then hydrated at certain temperatures by acidic, neutral and alkaline solutions.

reveal a negative correlation between the diameters of DLPC-based MFs and the pH of the aqueous medium. This tendency coincides with that previously observed for structures composed of DMPC. A comparison of the diameters of DLPC- and DMPC-based MFs grown under the same pH conditions shows that predominantly lower values are observed for the MFs consisting of DLPC. It may be related to the fact that DLPC has fewer carbon atoms per chain than DMPC (12 vs. 14 carbons in its acyl chains), resulting in differences in structural parameters, such as an average thickness of fully hydrated lipid bilayers (e. g. 3.26 nm and 3.67 nm at 25 °C, respectively [70]). Although follow-up studies using cryo-transmission electron microscopy or SAXS would be helpful to obtain information on the thickness of lipid bilayers within as-prepared MFs, our results provide preliminary insight into modifying MF's properties in a widely available non-invasive way.

3.3. Imaging of MF morphology by one-photon excited fluorescence microscopy

Then, CFM was applied to gain insights into the morphology of MFs. For this purpose, the stock solution of phospholipids was stained with Nile Red, which exhibits strong red fluorescence in a medium rich in phosphatidylcholines [71,72]. Initially, it was experimentally confirmed that fluorescence from the labeled DMPC matrix might be observed upon excitation at 488 nm at 30 °C. As depicted in Fig. S5†, the emission in the range of 580 nm – 650 nm could be collected from the lipid bilayers of samples prepared after adding the aqueous phase of pH 1 and 7. Although the emission spectra of Nile Red may shift due to the local environment [73,74], the fluorescence intensity remains similar in this range between samples prepared after adding acidic and neutral solutions. For the strongly alkaline character of the isotropic phase, the intensity was fairly low in the range of 580 nm – 650 nm. Moreover, the differences between the emission recorded in two channels, 560 nm – 610 nm and 610 nm – 660 nm, were detected for MFs formed at pH 13

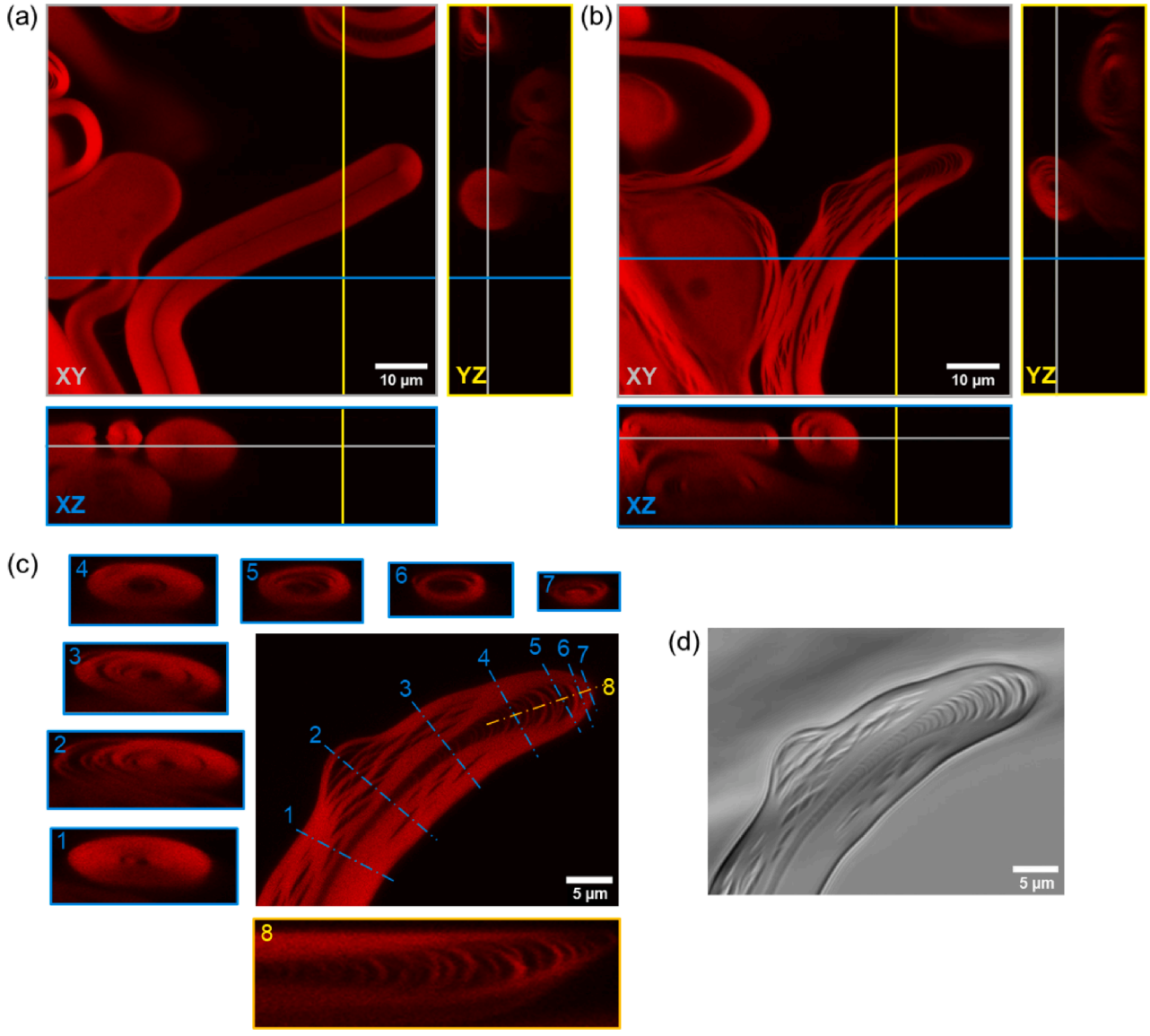

Fig. 3. (a) The confocal fluorescence microscopy images of DMPC-based MFs stained with Nile Red formed in the acidic medium (pH 1) at 30.0 °C. (b) Image of the same area of the sample taken after the process of cooling to 27.5 °C. The cross-sectional views were taken along blue and yellow lines in the planes perpendicular to the XY plane (marked in grey lines). (c) The corresponding 3D morphology analysis and (d) bight field image of the MF. The dashed blue and yellow cutting plane lines depict the spatial locations at which the cross-sectional views perpendicular to the XY plane are taken. The excitation was set at 488 nm (linearly polarized probe beam) and emission was collected between 580 and 650 nm. See also Fig. S7 and Fig. S8.

(Fig. S6†). As expected, there was no fluorescence signal from the water core in the first channel, but the signal of the same region was observed in the second channel, which was not noticed in other samples. Because the further study aimed to investigate the phase transition of MFs, and $T_{m\ DMPC}$ in neutral and strongly alkaline media is at a similar level (~24 °C), the following experiments were performed only for samples formed at pH of 1 and 7.

The use of a strongly acidic environment allowed us to raise the $T_{m\ DMPC}$ above RT, which facilitates detailed research on the formation of multilamellar lipid tubes. The growth of labeled DMPC-based MFs formed at the water phase of pH 1 was followed during the heating process that began 15 min after sample hydration (Video S1). Interestingly, non-emitting water channels were observed for elongated structures protruding from the edge of the lipid droplet. This suggests that the wetted DMPC-based film incubated below T_m might partially detach from the substrate. In this case, the membrane tension is lower than in the samples, where the dried lipid source is above its T_m at RT and remains attached to the microscope glass during the formation of MFs [75–77].

To provide spatial information on the multilamellar structures, the MFs were analyzed in three dimensions. For this purpose, the z-stack confocal images were obtained by scanning through the sample with the step of 0.3 μm, thus yielding smooth cross-sectional views (Fig. 3). As depicted in Fig. 3a and Fig. S7†, the representative straight DMPC-based MF formed in the acidic medium at 30 °C is the elongated structure with the oval cross-section and rod-like ending. Furthermore, it has a cylindrical lipid-free space that extends along the entire length of the tube. The volume and surface of its walls, consisting of coaxially aligned lipid

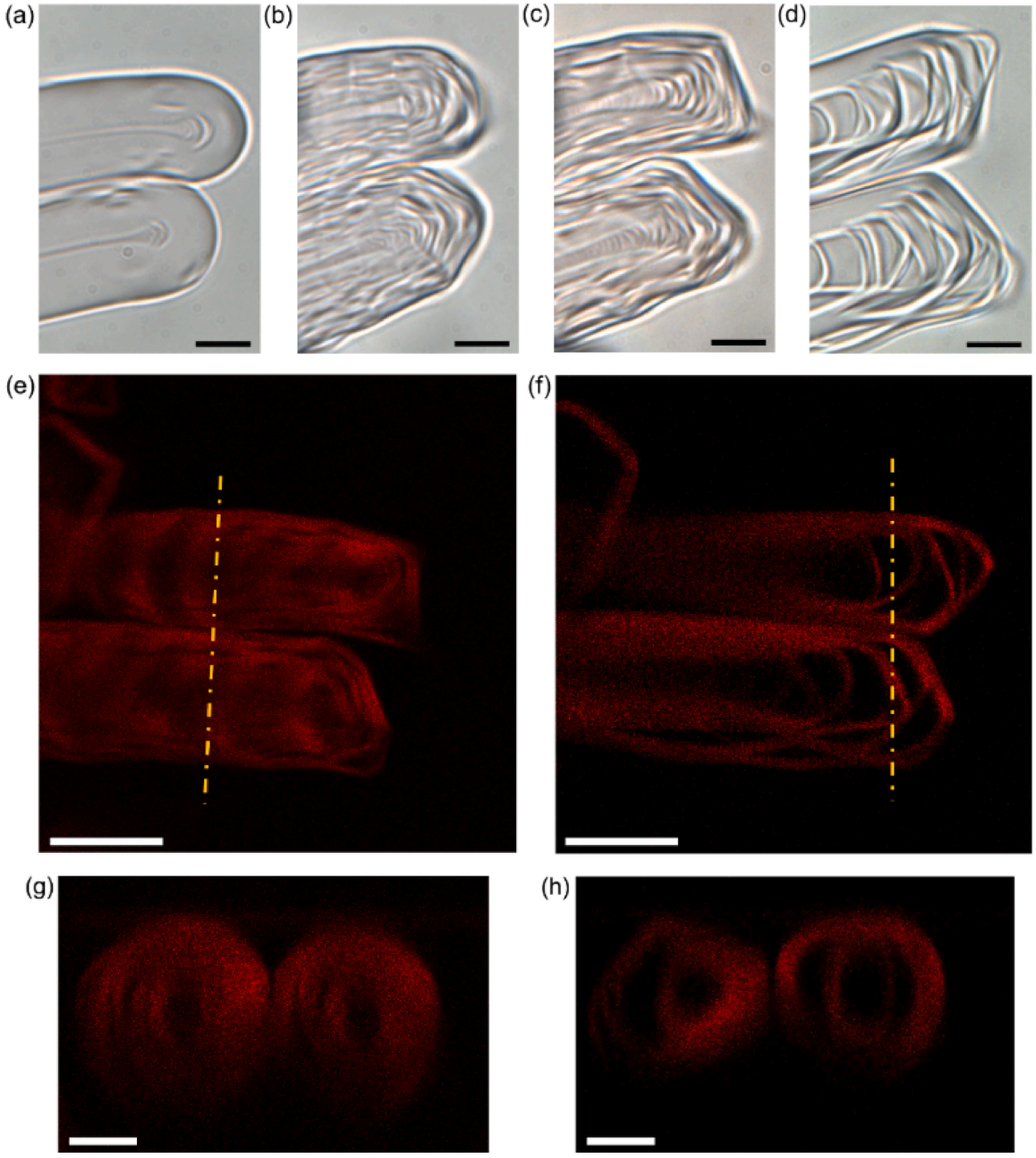

Fig. 4. (a-d) The bright field images of DMPC-based MFs with Nile Red performed during the cooling process from (a) 32.0 °C to (b-d) 27.5 °C. The images were taken (b) 30 s, (c) 5 min and (d) 50 min after reaching the temperature of 27.5 °C on the heating stage. (e, f) Two-photon excited fluorescence microscopy scans corresponding to (c) and (d), respectively (λ_{ex} = 980 nm, λ_{em}: 570 nm–685 nm). (g, h) The cross-sectional views were taken along the dashed yellow lines marked in (e) and (f), respectively. The scale bars represent (a-d, g, h) 5 μm and (e, f) 10 μm.

bilayers, are free of irregularities, such as changes in the diameters or arrangement of the lamellae. Fig. 3b shows the same area of the sample after the cooling process from 30.0 °C to 27.5 °C. Longitudinal areas of material loss of 2–4 μm were observed along the walls of the MF, and localized bulges of the structure were noted in the parts with high defect density. Previous studies have established that the cooling process of DLPC-based MFs can induce the formation of surface lesions along the entire length of the tube and the growth of lateral lipid tubes [77]. Here, defects appeared in the whole volume of the sample, and no branched structures were found. These structural changes reflect that the volume defects in the sample with DMPC result from lipid phase transition, whereas, in the experiments with DLPC, they are related to alterations in membrane fluidity above T_m.

Comparing the end of the representative MF above and below T_m demonstrates that the tip can tremble at 30.0 °C while it remains fixed at 27.5 °C (Fig. 3c and Fig. S7†). At lower temperatures, the tip adopts a sharper shape and points upward. What is more, in the front part of the tube, no longitudinal defects but delamination of the tip was distinguished (Fig. 3c, d). The farther away from the tip the thinner the region from which emission is collected. In both cases, the elongated part of the MF remains still during the scan along the z-axis. The diameter of the aqueous channel at 27.5 °C increases compared to the structure obtained at 30.0 °C, from approximately 0.2–0.4 μm to 0.8–0.9 μm (out of 30 measurements). Between the scans taken under these two temperature conditions, no significant changes were found in the collected emission signals. As shown in both fluorescence intensity plot profiles (Fig. S8†), the emission intensity decreases steadily (~20–30 %) from the edge to the core of the lipid tube.

3.4. Imaging of MF morphology by two-photon excited fluorescence microscopy

Further characterization was carried out using two-photon excited fluorescence imaging with the excitation wavelength set at 980 nm. Thus, the Nile Red molecules were excited by the absorption of 2 times lower energy photons than in the above-mentioned CFM experiments, which is essential for high-resolution non-invasive bioimaging [78–80]. Fig. 4a-d depict the phase behavior of MFs during the decrease in the temperature of the sample from 32 °C to 27.5 °C. The 2PEFM was used to take scans of the structures obtained 5 and 50 min after the heater objective reached 27.5 °C (Fig. 4e, f). The transverse cross-sectional views of the MFs reveal a circular shape, indicating a cylindrical structure of the lipid tube (Fig. 4g). After a longer incubation at 27.5 °C, the cross-sectional view of the MFs takes an oval shape and the water core is wider (Fig. 4h). The water core and wall defects are observed along the length of MFs, while larger areas of non-emitting phase are found towards the front of the tube. In both phases, the distribution of the lipid-free volume within the sample is qualitatively consistent with that observed with the CFM. These findings extend previous studies on fluorescence imaging of the aqueous phase within MFs marked with strongly emitting carbon nanodots [81].

Subsequently, we analyzed the alignment direction of lipids in multilamellar structures. While the Nile Red molecules are oriented parallel to the hydrophobic chains of lipids, this dye offers the possibility of indirectly determining the orientation of phosphatidylcholines in MFs [82–84]. The samples were scanned with a linearly polarized excitation beam, whose polarization direction was rotated from 0° to 270°. First, the structures obtained upon hydration of the DMPC droplet at 30 °C with the aqueous solution of pH 1 were investigated after cooling them to 27.5° C. The scans were taken with various polarizations (Fig. 5a), which depict differences in the location of the brightest and darkest areas of cylindrical structures. The most pronounced changes in emission intensity appeared at the edge of the sample and the delaminations closest to the front of the tube. Meanwhile, no differences have been observed inside the lipid tube. It suggests an altered long-range orientation of hydrophobic tails of the phospholipids relative to the MF water core below the phase transition temperature. As shown in Fig. S9†, 2PFEM could be used to determine the lipid alignment distribution in structures where PLM is insufficient (e.g. due to too low resolution). Subsequently, the MFs that occurred after the addition of the pH 7 water phase were examined under the same temperature conditions as in the previous sample. Depending on the polarization of the incident laser beam, distinct areas of varying emission intensity are observed along the MFs, except for the non-fluorescent core (Fig. 5b). The emission intensity variations indicate that the DMPC molecules are oriented perpendicular to the lipid-free volume running inside the MFs investigated above T_m.

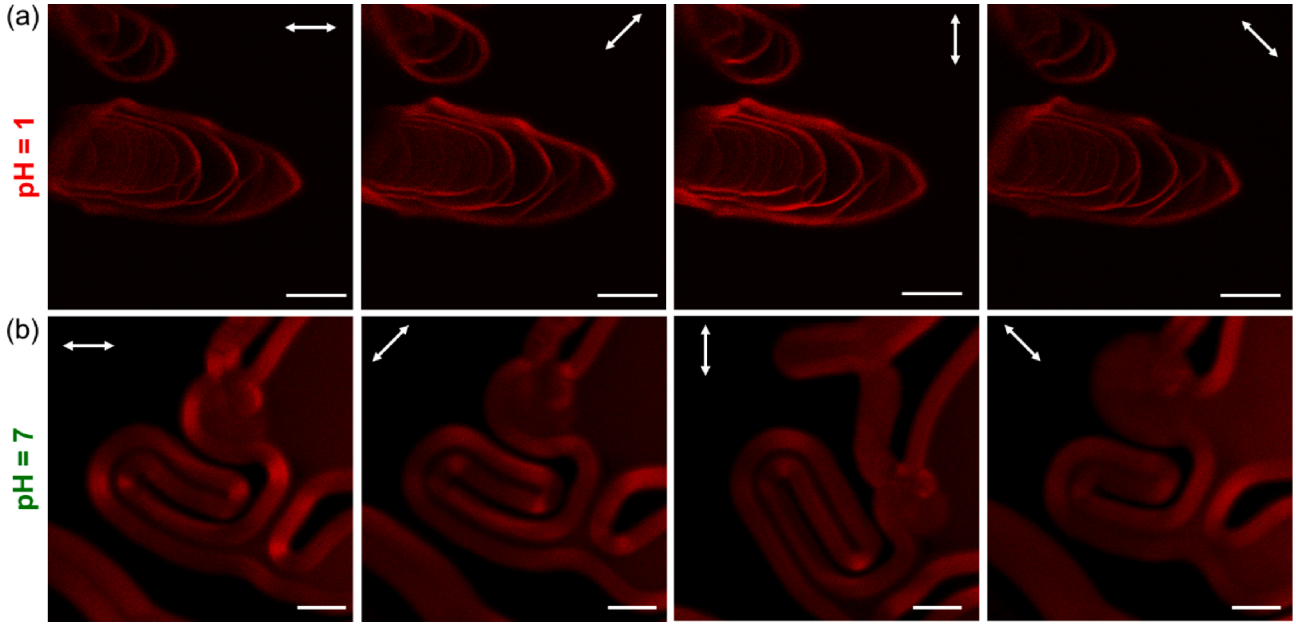

Fig. 5. The two-photon excited fluorescence microscopy images of DMPC-based MFs stained with Nile Red at 27.5 °C formed after the addition of the aqueous phase of (a) pH 1 and (b) pH 7. Both samples were heated to 30.0 °C and then cooled to 27.5 °C (λ_{ex} = 980 nm, λ_{em}: 570 nm–685 nm). The white double arrows indicate the orientation of laser beam's polarization directions (rotated within 0°−270°). Scale bars represent 10 μm.

4. Conclusion

We have demonstrated the significant effect of pH on the formation and morphology of single-component PC-based MFs using polarized light and fluorescence imaging techniques. Our research shows that precise control of the environment in which elongated multilayered microstructures consisting of saturated PCs are formed and tested is vital to design their properties. It was confirmed that there is a negative correlation between T_m and pH, which may result from varying charge of the lipid headgroup. In addition, the size of the MF was found to be strongly dependent on the initial conditions of the isotropic phase, showing a decreasing tendency of diameter with increasing pH. Besides, the following growth process over a wide range of pH values led us to conclude that the acidic medium facilitates the elongation of MFs. The change in the growth rate of MFs can be related to the reduced interfacial tension of lipid bilayers at low pH.

Moreover, this study provides valuable insights into the lipid phase transition within MFs. The 3D imaging performed by CFM revealed volume defects and delamination of the MF tip below T_m. Using 2PEFM, we successfully showed the orientational order of lipids within MFs at different conditions. From a material point of view, we have presented a material whose dimensions can be modified by the initial pH, while maintaining its elongated well-ordered microstructure for potential use as an optical waveguide as well as a matrix to organize small-scale dopants. Further detailed analysis of more complex models, using the microscopic techniques proposed here, has the potential to better understand the origin of structural changes in the myelin sheath.

CRediT authorship contribution statement

D. Benkowska-Biernacka: Conceptualization, Methodology, Investigation, Data curation, Visualization, Formal analysis, Writing – original draft. **I.I. Smalyukh:** Conceptualization, Resources, Writing – review & editing. **K. Matczyszyn:** Conceptualization, Resources, Writing – review & editing.

Declaration of Competing Interest

The authors declare that they have no known competing financial interests or personal relationships that could have appeared to influence the work reported in this paper.

Data availability

Data will be made available on request.

Acknowledgments

The authors thank T. Lee, S. Ghosh, A. Repula and H. Zhao for discussions and technical assistance. D.B.B. thanks M. Biernacki for the discussion on statistical analysis and M. Grzymajlo for technical assistance with DSC experiments. I.I.S. also acknowledges the support of the US National Science Foundation (DMR-1810513), including in terms of the utilized imaging instrumentation. The authors acknowledge the funding from the Polish National Science Centre (OPUS DEC/2019/35/B/ST4/03280). I.I.S. acknowledges hospitality of the International Institute for Sustainability with Knotted Chiral Meta Matter ($SKCM^2$) at Hiroshima University during his sabbatical visits, where he was partly discussing research findings related to this article.

Appendix A. Supplementary data

Supplementary information. Polarized light microscopy imaging of the formation of DMPC-based MFs in acidic and neutral media (Fig. S1†); observation of DMPC-based myelin figures phase transition during cooling and heating through T_m by polarized light microscopy (Fig. S2†); preparation and thermal analysis of DMPC-multilamellar vesicles (Fig. S3†); time evolution of the average diameter of DMPC-based myelin figures (Fig. S4†); polarized light microscopy images and corresponding confocal fluorescence images of myelin figures formed at acidic and neutral conditions (Fig. S5†); the confocal micrographs of DMPC-based MFs formed in alkaline solution (Fig. S6†); the three-dimensional analysis of confocal images of DMPC-based myelin formed above the phase transition temperature (Fig. S7†), the fluorescence intensity plot profiles of myelin figures (Fig. S8†); polarized light and two-photon microscopy imaging of DMPC-based myelin figures formed below the phase transition temperature (Fig. S9†) **PDF.** The time-lapse (1 frame per 3.22 s) confocal imaging of myelin figures formation (Video S1). **MP4** Supplementary data to this article can be found online at https://doi.org/10.1016/j.molliq.2023.123365.

References

[1] W.-S. Kim, J.-H. Im, H. Kim, J.-K. Choi, Y. Choi, Y.-K. Kim, Liquid crystalline systems from nature and interaction of living organisms with liquid crystals, Adv. Mater. 35 (4) (2023) 2204275.
[2] J.X. Tang, Opportunities and challenges in biological soft matter research, Front. Soft Matter 2 (2022).
[3] R. Mezzenga, J.M. Seddon, C.J. Drummond, B.J. Boyd, G.E. Schröder-Turk, L. Sagalowicz, Nature-inspired design and application of lipidic lyotropic liquid crystals, Adv. Mater. 31 (35) (2019) 1900818.
[4] R. Shaharabani, M. Ram-On, R. Avinery, R. Aharoni, R. Arnon, Y. Talmon, R. Beck, Structural transition in myelin membrane as initiator of multiple sclerosis, J. Am. Chem. Soc. 138 (37) (2016) 12159–12165.
[5] C. Binot, C.H. Chouard, Neurodegenerative diseases, infectious pathologies and liquid crystals: Hypothesis of a common information vector involving a multidisciplinary approach, Rev. Neurol. 174 (7) (2018) 540–554.
[6] J. Mahamid, D. Tegunov, A. Maiser, J. Arnold, H. Leonhardt, M. Plitzko Jürgen, W. Baumeister, Liquid-crystalline phase transitions in lipid droplets are related to cellular states and specific organelle association, Proc. Natl. Acad. Sci. 116(34) (2019) 16866-16871.
[7] L.-N. Zou, S.R. Nagel, Stability and Growth of Single Myelin Figures, Phys. Rev. Lett. 96 (13) (2006), 138301.
[8] A. Kister, I. Kister, Overview of myelin, major myelin lipids, and myelin-associated proteins, Front. Chem. 10 (2023).
[9] D.W. Lee, Y. Min, P. Dhar, A. Ramachandran, J.N. Israelachvili, J.A. Zasadzinski, Relating domain size distribution to line tension and molecular dipole density in model cytoplasmic myelin lipid monolayers, Proc. Natl. Acad. Sci. 108(23) (2011) 9425-9430.
[10] B. Krugmann, A. Koutsioubas, L. Haris, S. Micciulla, D. Lairez, A. Radulescu, S. Förster, A.M. Stadler, Adhesion process of biomimetic myelin membranes triggered by myelin basic protein, Front. Chem. 9 (2021).
[11] W. Teo, A.V. Caprariello, M.L. Morgan, A. Luchicchi, G.J. Schenk, J.T. Joseph, J.J. G. Geurts, P.K. Stys, Nile Red fluorescence spectroscopy reports early physicochemical changes in myelin with high sensitivity, Proc. Natl. Acad. Sci. USA 118(8) (2021).
[12] S. Andrade, M.J. Ramalho, J.A. Loureiro, M.C. Pereira, Liposomes as biomembrane models: Biophysical techniques for drug-membrane interaction studies, J. Mol. Liq. 334 (2021), 116141.
[13] J.N. Israelachvili, D.J. Mitchell, B.W. Ninham, Theory of self-assembly of lipid bilayers and vesicles, BBA 470 (2) (1977) 185–201.
[14] T. Sych, Y. Mély, W. Römer, Lipid self-assembly and lectin-induced reorganization of the plasma membrane, Philos. Trans. R. Soc., B 373 (1747) (2018) 20170117.
[15] H. Chen, M.-H. Li, Recent progress in polymer cubosomes and hexosomes, Macromol. Rapid Commun. 42 (15) (2021) 2100194.
[16] B.N. Thomas, C.R. Safinya, R.J. Plano, N.A. Clark, Lipid tubule self-assembly: length dependence on cooling rate through a first-order phase transition, Science (New York, N.Y.) 267 (1995) 1635–1638.
[17] M.J. Hope, M.B. Bally, L.D. Mayer, A.S. Janoff, P.R. Cullis, Generation of multilamellar and unilamellar phospholipid vesicles, Chem. Phys. Lipids 40 (2) (1986) 89–107.
[18] I. Sakurai, T. Suzuki, S. Sakurai, Cross-sectional view of myelin figures, Biochimica et Biophysica Acta (BBA) - Biomembranes 985 (1) (1989) 101–105.
[19] J.C.S. Ho, W.-C. Su, X. Chun Wang, A.N. Parikh, B. Liedberg, Nonequilibrium self-organization of lipids into hierarchically ordered and compositionally graded cylindrical smectics, Langmuir 38 (3) (2022) 1045–1056.
[20] J.F. Nagle, Theory of the main lipid bilayer phase transition, Annu. Rev. Phys. Chem. 31 (1) (1980) 157–196.
[21] K.M.G. Taylor, R.M. Morris, Thermal analysis of phase transition behaviour in liposomes, Thermochim Acta 248 (1995) 289–301.
[22] S. Youssefian, N. Rahbar, C.R. Lambert, S. Van Dessel, Variation of thermal conductivity of DPPC lipid bilayer membranes around the phase transition temperature, J. Royal Soc. Interface 14 (130) (2017).
[23] D. Drabik, G. Chodaczek, S. Kraszewski, M. Langner, Mechanical Properties Determination of DMPC, DPPC, DSPC, and HSPC Solid-Ordered Bilayers, Langmuir 36 (14) (2020) 3826–3835.

[24] N. Färber, C. Westerhausen, Broad lipid phase transitions in mammalian cell membranes measured by Laurdan fluorescence spectroscopy, Biochim. Biophys. Acta 1864 (1) (2022), 183794.
[25] F. Tokumasu, A.J. Jin, J.A. Dvorak, Lipid membrane phase behaviour elucidated in real time by controlled environment atomic force microscopy, J. Electron Microsc. 51 (1) (2002) 1–9.
[26] N. Kučerka, M.-P. Nieh, J. Katsaras, Fluid phase lipid areas and bilayer thicknesses of commonly used phosphatidylcholines as a function of temperature, Biochimica et Biophysica Acta (BBA) - Biomembranes 1808 (11) (2011) 2761–2771.
[27] S. Šegota, D. Vojta, G. Pletikapić, G. Baranović, Ionic strength and composition govern the elasticity of biological membranes. A study of model DMPC bilayers by force- and transmission IR spectroscopy, Chem. Phys. Lipids 186 (2015) 17–29.
[28] V.A. Magnotta, H.-Y. Heo, B.J. Dlouhy, N.S. Dahdaleh, R.L. Follmer, D.R. Thedens, M.J. Welsh, J.A. Wemmie, Detecting activity-evoked pH changes in human brain, Proc. Natl. Acad. Sci. 109(21) (2012) 8270-8273.
[29] A. Jagielska, K.D. Wilhite, K.J. Van Vliet, Extracellular acidic pH inhibits oligodendrocyte precursor viability, migration, and differentiation, PLoS One 8 (9) (2013) e76048.
[30] S.M. Theparambil, P.S. Hosford, I. Ruminot, O. Kopach, J.R. Reynolds, P. Y. Sandoval, D.A. Rusakov, L.F. Barros, A.V. Gourine, Astrocytes regulate brain extracellular pH via a neuronal activity-dependent bicarbonate shuttle, Nat. Commun. 11 (1) (2020) 5073.
[31] D. Kuzman, T. Žnidarčič, M. Gros, S. Vrhovec, S. Svetina, B. Žekš, Effect of pH on red blood cell deformability, Pflügers Archiv – Eur. J. Physiol. 440 (1) (2000) R193–R194.
[32] Y. Lee, D.H. Thompson, Stimuli-responsive liposomes for drug delivery, Wiley interdisciplinary reviews, Nanomed. Nanobiotechnol. 9 (5) (2017).
[33] R. Negrini, R. Mezzenga, pH-responsive lyotropic liquid crystals for controlled drug delivery, Langmuir 27 (9) (2011) 5296–5303.
[34] P. Garidel, C. Johann, L. Mennicke, A. Blume, The mixing behavior of pseudobinary phosphatidylcholine-phosphatidylglycerol mixtures as a function of pH and chain length, Eur. Biophys. J. 26 (6) (1997) 447–459.
[35] M.B. Boggara, R. Krishnamoorti, Small-Angle Neutron Scattering Studies of Phospholipid−NSAID Adducts, Langmuir 26 (8) (2010) 5734–5745.
[36] A. Chowdhury, S. Sasidharan, P. Xavier, P. Viswanath, V.A. Raghunathan, Effect of pH on the phase behavior of DMPC bilayers, Biochimica et Biophysica Acta (BBA) -, Biomembranes 1863 (11) (2021), 183695.
[37] M. Anderson, A. Omri, The effect of different lipid components on the in vitro stability and release kinetics of liposome formulations, Drug Deliv. 11 (1) (2004) 33–39.
[38] R.N. Lewis, D.A. Mannock, R.N. McElhaney, Differential scanning calorimetry in the study of lipid phase transitions in model and biological membranes: practical considerations, Methods in molecular biology (Clifton, N.J.) 400 (2007) 171–195.
[39] P.V. Konarev, A.Y. Gruzinov, H.D.T. Mertens, D.I. Svergun, Restoring structural parameters of lipid mixtures from small-angle X-ray scattering data, J. Appl. Cryst. 54 (Pt 1) (2021) 169–179.
[40] Z. Brkljača, M. Ćehić, T. Portada, M. Butumović, D. Bakarić, I. Crnolatac, Monitoring lipid phase transition temperatures using fluorescent probes and temperature-dependent fluorescence spectroscopy, Dyes Pigm. 206 (2022), 110621.
[41] W. Chen, F. Duša, J. Witos, S.K. Ruokonen, S.K. Wiedmer, Determination of the main phase transition temperature of phospholipids by nanoplasmonic sensing, Sci Rep 8 (1) (2018) 14815.
[42] L.A. Bagatolli, E. Gratton, Two-photon fluorescence microscopy observation of shape changes at the phase transition in phospholipid giant unilamellar vesicles, Biophys. J. 77 (4) (1999) 2090–2101.
[43] C.B. Fox, R.H. Uibel, J.M. Harris, Detecting phase transitions in phosphatidylcholine vesicles by Raman microscopy and self-modeling curve resolution, J. Phys. Chem. B 111 (39) (2007) 11428–11436.
[44] N. Kučerka, Y. Liu, N. Chu, H.I. Petrache, S. Tristram-Nagle, J.F. Nagle, Structure of fully hydrated fluid phase DMPC and DLPC lipid bilayers using X-ray scattering from oriented multilamellar arrays and from unilamellar vesicles, Biophys. J. 88 (4) (2005) 2626–2637.
[45] Y. Min, K. Kristiansen, J.M. Boggs, C. Husted, J.A. Zasadzinski, J. Israelachvili, Interaction forces and adhesion of supported myelin lipid bilayers modulated by myelin basic protein, PNAS 106 (9) (2009) 3154–3159.
[46] J.N. van der Veen, J.P. Kennelly, S. Wan, J.E. Vance, D.E. Vance, R.L. Jacobs, The critical role of phosphatidylcholine and phosphatidylethanolamine metabolism in health and disease, Biochimica et Biophysica Acta (BBA) - Biomembranes 1859(9, Part B) (2017) 1558-1572.
[47] K.-C. Lin, R.M. Weis, H.M. McConnell, Induction of helical liposomes by Ca2+-mediated intermembrane binding, Nature 296 (5853) (1982) 164–165.
[48] I. Sakurai, Y. Kawamura, Magnetic-field-induced orientation and bending of the myelin figures of phosphatidylcholine, Biochimica et Biophysica Acta (BBA) - Biomembranes 735 (1) (1983) 189–192.
[49] L.M. Amende, E.J. Blanchette-Mackie, S.S. Chernick, R.O. Scow, Effect of pH on visualization of fatty acids as myelin figures in mouse adipose tissue by freeze-fracture electron microscopy, Biochimica et Biophysica Acta (BBA) - Lipids and Lipid, Metabolism 837 (1) (1985) 94–102.
[50] K. Mishima, S. Nakamae, H. Ohshima, T. Kondo, Frequency dependence of electric-field-induced orientation of myelin tubes, Biochimica et Biophysica Acta (BBA) - Biomembranes 1191 (1) (1994) 157–163.
[51] H. Dave, M. Surve, C. Manohar, J. Bellare, Myelin growth and initial dynamics, J. Colloid Interface Sci. 264 (1) (2003) 76–81.
[52] D.J. Speer, J.C.S. Ho, A.N. Parikh, Surfactant-mediated solubilization of myelin figures: a multistep morphological cascade, Langmuir (2022).
[53] N. Fathi, A.-R. Moradi, M. Habibi, D. Vashaee, L. Tayebi, Digital holographic microscopy of the myelin figure structural dynamics and the effect of thermal gradient, Biomed. Opt. Express 4 (6) (2013) 950–957.
[54] R. Mosaviani, A.-R. Moradi, L. Tayebi, Effect of humidity on liquid-crystalline myelin figure growth using digital holographic microscopy, Mater. Lett. 173 (2016) 162–166.
[55] L.-N. Zou, Myelin figures: The buckling and flow of wet soap, Phys. Rev. E 79 (6) (2009), 061502.
[56] M. Allah Panahi, Z. Tahmasebi, V. Abbasian, M. Amiri, A.-R. Moradi, Role of pH level on the morphology and growth rate of myelin figures, Biomed. Opt. Express 11 (10) (2020) 5565–5574.
[57] T. Lee, R.P. Trivedi, I.I. Smalyukh, Multimodal nonlinear optical polarizing microscopy of long-range molecular order in liquid crystals, Opt. Lett. 35 (20) (2010) 3447–3449.
[58] H. Akoglu, User's guide to correlation coefficients, Turkish J. Emerg. Med. 18 (3) (2018) 91–93.
[59] C. Xiao, J. Ye, R.M. Esteves, C. Rong, Using Spearman's correlation coefficients for exploratory data analysis on big dataset, Concurr. Comput.: Practice Experience 28 (14) (2016) 3866–3878.
[60] S. Khodaparast, W.N. Sharratt, R.M. Dalgliesh, J.T. Cabral, Growth of myelin figures from parent multilamellar vesicles, Langmuir 37 (42) (2021) 12512–12517.
[61] B. Roy, P. Guha, R. Bhattarai, P. Nahak, G. Karmakar, P. Chettri, A.K. Panda, Influence of lipid composition, pH, and temperature on physicochemical properties of liposomes with curcumin as model drug, J. Oleo Sci. 65 (5) (2016) 399–411.
[62] J.-F. Tocanne, J. Teissié, Ionization of phospholipids and phospholipid-supported interfacial lateral diffusion of protons in membrane model systems, Biochimica et Biophysica Acta (BBA) - Reviews on Biomembranes 1031 (1) (1990) 111–142.
[63] K. Mishima, K. Yoshiyama, Growth rate of myelin figures of egg-yolk phosphatidylcholine, BBA 904 (1) (1987) 149–153.
[64] L. Reissig, D.J. Fairhurst, J. Leng, M.E. Cates, A.R. Mount, S.U. Egelhaaf, Three-dimensional structure and growth of Myelins, Langmuir 26 (19) (2010) 15192–15199.
[65] R. Taribagil, M.A. Arunagirinathan, C. Manohar, J.R. Bellare, Extended time range modeling of myelin growth, J. Colloid Interface Sci. 289 (1) (2005) 242–248.
[66] M. Haran, A. Chowdhury, C. Manohar, J. Bellare, Myelin growth and coiling, Colloids Surf. A Physicochem. Eng. Asp. 205 (1) (2002) 21–30.
[67] M. Buchanan, S.U. Egelhaaf, M.E. Cates, Dynamics of interface instabilities in nonionic lamellar phases, Langmuir 16 (8) (2000) 3718–3726.
[68] A.D. Petelska, Z.A. Figaszewski, Effect of pH on the interfacial tension of lipid bilayer membrane, Biophys. J. 78 (2) (2000) 812–817.
[69] K. Lähdesmäki, O.H.S. Ollila, A. Koivuniemi, P.T. Kovanen, M.T. Hyvönen, Membrane simulations mimicking acidic pH reveal increased thickness and negative curvature in a bilayer consisting of lysophosphatidylcholines and free fatty acids, Biochimica et Biophysica Acta (BBA) - Biomembranes 1798 (5) (2010) 938–946.
[70] R.A. Karjiban, N.S. Shaari, U.V. Gunasakaran, M. Basri, A coarse-grained molecular dynamics study of DLPC, DMPC, DPPC, and DSPC mixtures in aqueous solution, J. Chem. 2013 (2013) 1–6.
[71] P. Greenspan, S.D. Fowler, Spectrofluorometric studies of the lipid probe, nile red, J. Lipid Res. 26 (7) (1985) 781–789.
[72] G. Diaz, M. Melis, B. Batetta, F. Angius, A.M. Falchi, Hydrophobic characterization of intracellular lipids in situ by Nile Red red/yellow emission ratio, Micron (Oxford, England : 1993) 39(7) (2008) 819-24.
[73] D.L. Sackett, J. Wolff, Nile red as a polarity-sensitive fluorescent probe of hydrophobic protein surfaces, Anal. Biochem. 167 (2) (1987) 228–234.
[74] R. Mishra, D. Sjölander, P. Hammarström, Spectroscopic characterization of diverse amyloid fibrilsin vitro by the fluorescent dye Nile red, Mol. Biosyst. 7 (4) (2011) 1232–1240.
[75] L. Tayebi, M. Mozafari, D. Vashaee, A.N. Parikh, Structural configuration of myelin figures using fluorescence microscopy, Int. J. Photoenergy 2012 (2012), 685617.
[76] M. Simunovic, G.A. Voth, Membrane tension controls the assembly of curvature-generating proteins, Nat. Commun. 6 (1) (2015) 7219.
[77] D. Benkowska-Biernacka, I.I. Smalyukh, K. Matczyszyn, Morphology of lyotropic myelin figures stained with a fluorescent dye, J. Phys. Chem. B 124 (52) (2020) 11974–11979.
[78] P. Sahu, N. Mazumder, Advances in adaptive optics–based two-photon fluorescence microscopy for brain imaging, Lasers Med. Sci. 35 (2) (2020) 317–328.
[79] Z. Qin, S. He, C. Yang, J.-S.-Y. Yung, C. Chen, C.-K.-S. Leung, K. Liu, J.Y. Qu, Adaptive optics two-photon microscopy enables near-diffraction-limited and functional retinal imaging in vivo, Light Sci. Appl. 9 (1) (2020) 79.
[80] M. Hornum, P. Reinholdt, J.K. Zaręba, B.B. Jensen, D. Wüstner, M. Samoć, P. Nielsen, J. Kongsted, One- and two-photon solvatochromism of the fluorescent dye Nile Red and its CF3, F and Br-substituted analogues, Photochem. Photobiol. Sci. 19 (10) (2020) 1382–1391.
[81] D. Benkowska-Biernacka, S.G. Mucha, L. Firlej, F. Formalik, J.-L. Bantignies, E. Anglaret, M. Samoć, K. Matczyszyn, Strongly emitting folic acid-derived carbon nanodots for one- and two-photon imaging of lyotropic myelin figures, ACS Appl. Mater. Interfaces (2023).

[82] I.I. Smalyukh, Confocal microscopy of director structures in strongly confined and composite systems, molecular crystals and liquid crystals 477(1) (2007) 23/[517]-41/[535].
[83] B. Jana, S. Ghosh, N. Chattopadhyay, Competitive binding of nile red between lipids and β-cyclodextrin, J. Photochem. Photobiol. B Biol. 126 (2013) 1–10.
[84] J. Rumin, H. Bonnefond, B. Saint-Jean, C. Rouxel, A. Sciandra, O. Bernard, J.-P. Cadoret, G. Bougaran, The use of fluorescent Nile red and BODIPY for lipid measurement in microalgae, Biotechnol. Biofuels 8 (1) (2015) 42.